

# Digital Research on the Influence of Longitudinal Zone on the Adjustment of Threshold Crossing Height

Chunqing Qu<sup>1,2</sup>

<sup>1</sup>Equipment Operation Monitoring Center, East China Regional Air Traffic Management Bureau of Civil Aviation of China, CAAC, Shanghai, China

<sup>2</sup>Digitalization Innovative Laboratory, East China Regional Air Traffic Management Bureau of Civil Aviation of China, CAAC, Shanghai, China

Email: qcq04@163.com

**How to cite this paper:** Qu, C.Q. (2025) Digital Research on the Influence of Longitudinal Zone on the Adjustment of Threshold Crossing Height. *Open Journal of Applied Sciences*, 15, 3478-3488. <https://doi.org/10.4236/ojapps.2025.1511224>

**Received:** October 14, 2025

**Accepted:** November 2, 2025

**Published:** November 5, 2025

Copyright © 2025 by author(s) and Scientific Research Publishing Inc. This work is licensed under the Creative Commons Attribution International License (CC BY 4.0).

<http://creativecommons.org/licenses/by/4.0/>



Open Access

## Abstract

Antenna rotation is studied for the adjustment of Threshold Crossing Height (TCH) in longitudinal terrain. The TCH value radiated from the M array Glide Path (GP) beacon can be raised or lowered flexibly. This effect originates from the structure adjustment of the glide slope in the near field (NF) by a rotation of the upper antenna horizontal from reverse rotation  $\phi = -10^\circ$  to forward rotation  $\phi = +10^\circ$ . Except for the situation with a series of backward distances from  $d = 100$  m to 600 m with an interval of 100 m under standard terrain, the uphill from forward slope (*FSL*)  $FSL = +2^\circ$  to the downhill  $FSL = -2^\circ$  with a gap of one degree has been systematically and digitally researched. The bias setting of the GP beacon would be optimized automatically to meet different terrain requirements. The rule of the Threshold Crossing Height and the variety of TCH ( $\Delta T$ ) corresponding to  $d$  and *FSL* have been revealed. The strong correlation between  $\Delta T$  and *FSL* can be applied to site selection during the initial stage of runway construction.

## Keywords

Forward Slope, Drawback Distance, Threshold Crossing Height

## 1. Introduction

The Instrument Landing System (ILS) [1]-[3] plays an important part in civil aviation and has become the international standard system for approach and landing guidance. Its combination of Glide Path [4] [5] (GP) and Distance

Measuring Equipment (DME) [6] can supply vertical guidance and provide a precise approach for aircraft. Threshold Crossing Height (TCH) works as a critical parameter in the glide path system. The magnitude of TCH values mainly depends on the near-field (NF) signal, especially the structure of the Difference in Depth of Modulation (DDM) in Zone III, rather than being determined by the far-field (FF) signal. For the field in front of the antenna array, the longitudinal distance directly affects the variation of TCH. And the change in forward slope causes a change in height of antennas, resulting in the readjustment of a series of parameters such as forward shift and lateral bias of the antennas. Technicians have conducted extensive research on the methods of TCH adjustment, including altering antenna height, changing the lateral offset of the upper and lower antennas, and the most effective method is to rotate the antenna [7]. However, there is little research on the impact of terrain on TCH. This article explores the factors related to longitudinal terrain: the rule of variation of  $\Delta T$  by antenna rotation, as well as TCH with drawback distances  $d$  and forward slopes  $FSL$ .

## 2. Methods

### 2.1. Antenna Foundation

The typical installation position of the glide slide antenna is 300 m away from the runway entrance and 120 m away from the centerline of the runway, as shown by the red dot in **Figure 1**. The two main factors studied in the longitudinal zone are the drawback distance ( $d$ ) and the forward slope ( $FSL$ ). The study range of the drawback distance is from  $d = 100$  m to  $d = 600$  m. The region of reflective surface is the flat ground in common, namely,  $FSL = 0^\circ$ . The purple area in **Figure 1** represents the reflection zone in front of the Gilde Path antenna system, and the range of forward slope considered is from  $FSL = -2^\circ$  to  $FSL = +2^\circ$ . The six positions of the Gilde Path beacon are the test positioning points. There are three Kathrein [8] antennas of the M array glide path antenna [9], the lower antenna in green, the middle antenna in yellow, and the upper antenna in purple. For each point, the upper antenna of the beacon would rotate to and away from the runway ten degrees. Define the corner position  $\phi_r$  from the front of the test point to the T point [10] of the runway entrance.

The antennas excitation amplitudes and phases are listed in **Table 1**.

**Table 1.** Signal distribution of M-type glide path antenna.

	CSB	SBO	CL
Upper Ant	Null	90 Hz $0.059 * A(\phi) \angle 0^\circ$ 150 Hz $0.059 * A(\phi) \angle 180^\circ$	150 Hz $0.2 * A(\phi) \angle 0^\circ$
Middle Ant	$0.5 \angle 180^\circ$	90 Hz $0.117 \angle 180^\circ$ 150 Hz $0.117 \angle 0^\circ$	Null
Lower Ant	$1.0 \angle 0^\circ$	90 Hz $0.059 \angle 0^\circ$ 150 Hz $0.059 \angle 180^\circ$	150 Hz $0.2 \angle 0^\circ$

The factors that ground conductivity and soil moisture have a slight impact on the reflection coefficient  $\Gamma$ , but it has almost no effect on signal synthesis at small reflection angles around 3 degrees. Assuming that the reflecting surface is a good conductor, the reflection coefficient  $\Gamma = 1.00$ , and the signal is totally reflected.

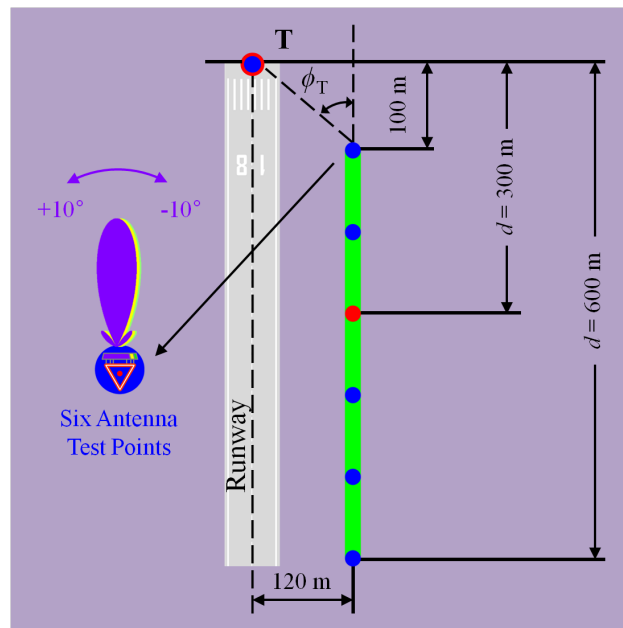


**Figure 1.** (Color online) Locations and test position of the Gilde Path beacon. The blue points are a series of testing positions from the drawback distance  $d = 100$  m to  $d = 600$  m. The red point is the typical location with lateral distance  $l = 120$  m and drawback distance  $d = 300$  m.  $\phi_T$  is the angle from the testing point of the antenna to the threshold crossing height on the horizontal plane. For each test point, the upper antenna can rotate horizontally within  $\pm 10$  degrees.

## 2.2. Bias Optimization

For situations with a forward slope, the height and lateral position of the three antennas need to be adjusted. When the reflection field in front of the antenna is uphill, the height of the antennas needs to be raised in order to hold a 3-degree elevation angle with the horizontal plane for the composite signal composed of direct and reflected signals, as seen in the side view of **Figure 2**. The original height of the lower antenna is  $h_0$ . And the adjusted height of the lower one is  $h'$ . The height adjustment method is given in Formula (1). The antennas need to be forward offset adjusted on the forward slope. To achieve the target of the antenna being perpendicular to the average forward slope, the antennas are set to the forward shift. For an uphill slope, that is,  $FSL > 0^\circ$ , keep the upper antenna stationary, and the lower and middle antennas are moved towards the direction of the threshold of the runway at a ratio of 2:1, seen in Formulas (2) and (3); the heights of the three antennas increase proportionally, as described in the side view of **Figure 2**. And for a downhill slope, namely  $FSL < 0^\circ$ , the antenna height

needs to be lowered. The upper and middle antennas are moved towards the direction of the threshold of the runway at a ratio of 2:1, and the lower antenna is stationary. The heights of the three antennas are reduced proportionally for an elevation larger than the Gilde Path angle, to ensure that the synthesized signal complies with the downhill remaining vertical at a  $3^\circ$  angle. The adjustment range of  $FSL$  is from uphill to  $+2$  degrees and downhill to  $-2$  degrees.

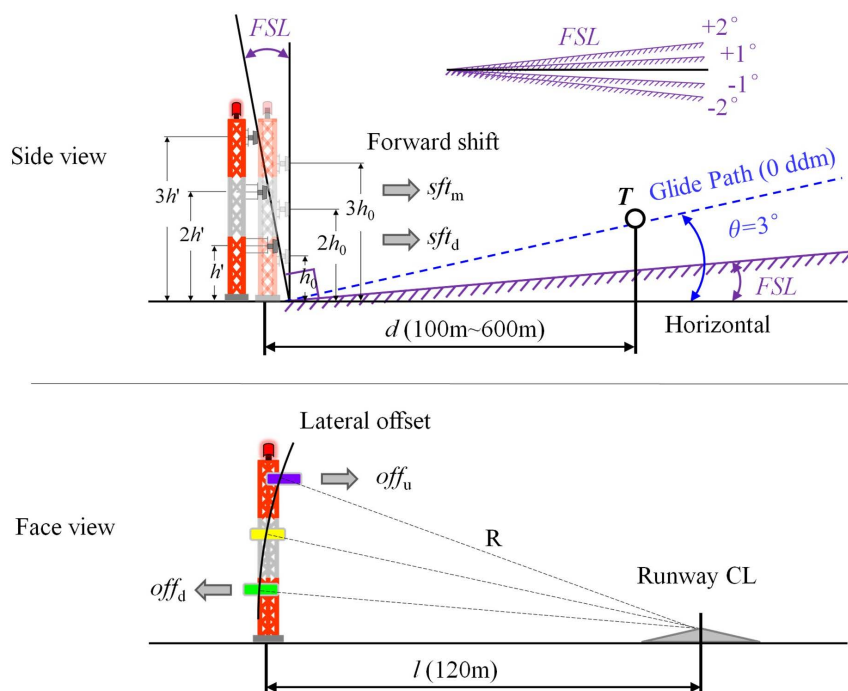


**Figure 2.** (Color online) Forward shift and Lateral offset of the M array Gilde Path system. The three antennas should be aligned along a straight line on the forward slope ( $FSL$ ), which shall be perpendicular to the average forward slope. In the case of  $FSL = 0^\circ$ , the three antennas focus on the same point in a top view. For an uphill slope, the lower antenna shall be forward compared to the middle antenna and the upper antenna. And the antenna's height should also be raised synchronously. To calibrate the phase difference from antennas to the center line of the runway, the upper antenna is closer to the runway than the middle antenna, and the middle antenna shall be closer to the runway than the lower antenna.

$$h' = \frac{c}{4f \sin(3^\circ - FSL)} \quad (1)$$

When  $FSL = 0^\circ$ ,  $h_0$  is 4.3 meters, corresponding to a transmission wavelength is 0.9 m and the corresponding frequency is 333.35 MHz.

$$sft_m = (h_u - h_m) \sin(FSL) = h' \sin(FSL) \quad (2)$$

$$sft_d = (h_u - h_d) \sin(FSL) = 2h' \sin(FSL) \quad (3)$$

To eliminate the phase error from three antennas to the center line of the runway, the actual operation method is to make the upper and lower antennas offset

in the opposite direction, seen in Formulas (4) and (5), with a lateral offset of 5:3, presented in the face view of **Figure 1**.

$$off_u = \frac{h_m^2 - h_u^2}{2l} = -\frac{5h'^2}{2l} \tag{4}$$

$$off_d = \frac{h_m^2 - h_d^2}{2l} = \frac{3h'^2}{2l} \tag{5}$$

### 2.3. Method to Achieve TCH

The 3D model is established by MATLAB, the frequency of the transmitter is taken as 333.35 MHz, the corresponding wavelength is 0.9 m. The drawback distance is 300 m and the lateral distance is 120 m. According to the flight checking procedure, the method to achieve the TCH is for the aircraft to continuously track the glide slope, collect the position of the points of ddm (0 ddm) point in the zone from 1830 m to 300 m horizontally away from the runway entrance, and fit the data of 0 ddm by the least squares method [11]. The value of the fitted curve extends to the runway entrance, and the position of the corresponding height is TCH. The DDM curves corresponding to the forward and reverse rotation of the upper antenna by 10 degrees are shown in **Figure 3**. The cyan dots are the zero-point positions of the DDM curves of two kinds of rotation.

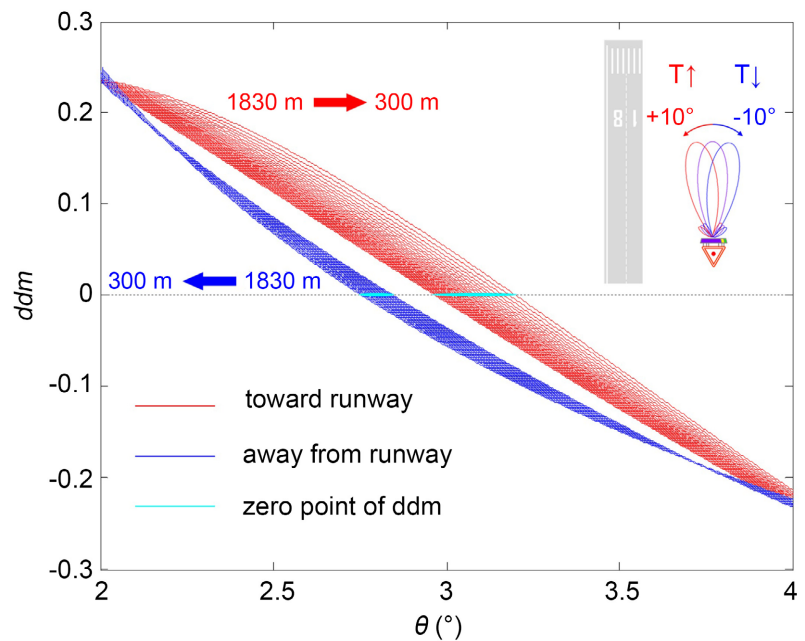


**Figure 3.** (Color online) *DDM* patterns of the upper antenna forward and reverse rotation. The blue curves represent the antenna rotating away from the runway, and the red ones represent the antenna rotating toward the runway. When the antenna turns to the runway, TCH rises. When the antenna turns outside the runway, TCH descends. The type of antenna is a Kathrein antenna. Its horizontal pattern owns a main lobe with a half-width of 25°.

Due to the design of a glide sliding angle of 3 degrees, the drawback distance

has a direct impact on the TCH. They have a strong correlation and exhibit extremely violent, regular changes. The drawback distance from 100 m to 600 m responding to TCH curves with different  $FSL$  from  $-2^\circ$  to  $+2^\circ$  is listed in **Figure 4**. It can be found that the TCH grows linearly with the increase in the drawback distance. Also, with the decrease in  $FSL$ , the TCH keeps increasing. The interval of TCH between each slope of  $FSL$  is almost identical for a series of drawback distances  $d$ . The adjustment effect of TCH decreases by 33% for every degree increase in  $FSL$ .

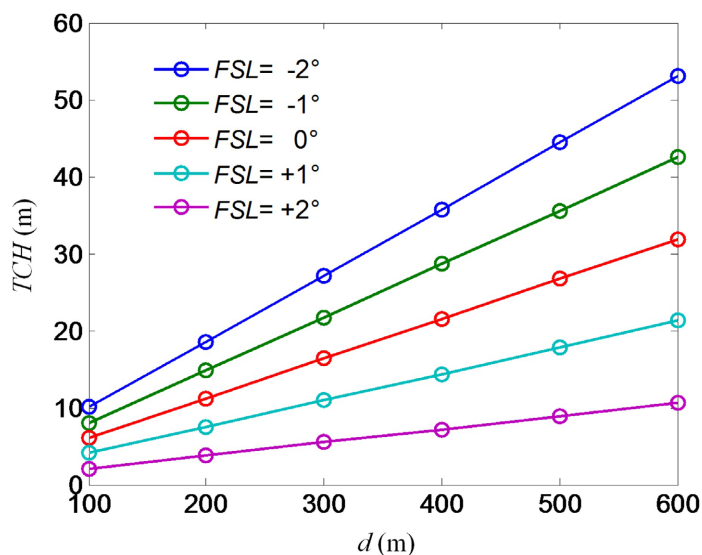


**Figure 4.** (Color online) TCH responds to the drawback distance  $d$  with a series of  $FSL$ .

#### 2.4. Theoretical Principle for Achieving Variation of TCH ( $\Delta T$ )

The TCH can be adjusted effectively by the upper antenna rotation [7]. Rotation of the upper antenna alone can effectively avoid affecting signal coverage. As seen in the insert in the upper right corner of **Figure 3**, the upper antenna rotates to the runway, the TCH raises, that is, forward rotation. On the contrary, the upper antenna rotates away from the runway, and the TCH descends, namely, reverse rotation. In the case of  $d = 300$  m with a flattened reflector, the  $\Delta T$  can reach approximately 2 meters by  $\phi = +10^\circ$  while  $-2.7$  meters by  $\phi = -10^\circ$ .

### 3. Results and Discussion

The two main parameters of longitudinal terrain are forward slope  $FSL$  and drawback distance  $d$ , and the response of variation of TCH ( $\Delta T$ ) by antenna rotation from  $\phi = -10^\circ$  to  $\phi = +10^\circ$  to longitudinal terrain is given in the following discussion. The  $\Delta T$  is positive by forward rotation of the upper antenna by  $\phi = +2^\circ, +4^\circ, +6^\circ, +8^\circ, +10^\circ$ . While the  $\Delta T$  is negative by reverse rotation of the upper antenna by  $\phi = -2^\circ, -4^\circ, -6^\circ, -8^\circ, -10^\circ$ . The larger the rotation angle, the greater the variation of TCH.

Considering the half-width with  $-3$  dB power (0.707 amplitude) of the Kathrein

lobe is  $12.5^\circ$ . Excessive rotation angle can lead to insufficient coverage. So, the rotation angle  $\phi$  in this study is restricted in  $\pm 10^\circ$  to ensure that the typical radiation power of 20 W can meet the glide path coverage requirements [10] with 18.5 Km within  $\pm 8^\circ$  in horizontal.

### 3.1. Forward Slope Responding

On a flat reflective surface, TCH decreases for reverse rotation by  $\phi = -10^\circ$  and  $\Delta T$  becomes negative, while TCH increases for forward rotation and  $\Delta T$  becomes positive. When  $d = 100$  m, the TCH can descend by more than 2 meters by  $\phi = -10^\circ$  and ascend by more than 2 meters by  $\phi = +10^\circ$ , as seen in the middle of **Figure 5**, for the case of  $FSL = 0^\circ$ . As  $d$  increases, the forward maximum value of  $\Delta T$  begins to decrease, while the reverse maximum value of  $\Delta T$  gradually increases. When  $d = 600$  m,  $\Delta T$  is approximately 1.4 m by  $\phi = +10^\circ$  while  $-3.1$  m by  $\phi = -10^\circ$ .

When the rotation angle  $\phi$  decreases, the correlation between  $\Delta T$  and  $d$  weakens, and the influence of  $\Delta T$  on  $d$  synchronously decreases. When the  $\phi$  is less than  $-5$  degrees for reverse rotation,  $\Delta T$  is almost unaffected by  $d$ . And when the  $\phi$  is larger than  $+3$  degrees for forward rotation, the relationship between  $\Delta T$  and  $d$  is not significant anymore.

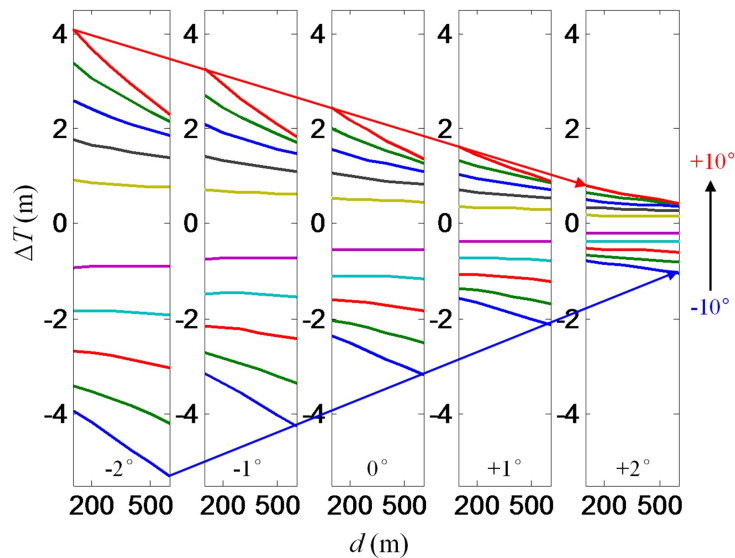


**Figure 5.** (Color online)  $\Delta T$  responds to  $d$  with a series of  $\phi$  from  $FSL = -2^\circ$  to  $+2^\circ$ .

When the forward slope appears, the above phenomenon still exists, but the difference is that the amplitude of  $\Delta T$  has changed. When  $FSL$  decreases, the amplitude proportion of  $\Delta T$  increases, while when  $FSL$  increases, the amplitude proportion of  $\Delta T$  decreases, as presented in **Figure 5**. The variation amplitude of  $FSL$  and  $\Delta T$  shows a good linear proportional relationship, as shown in the red line for the case of  $\phi = +10^\circ$  and  $d = 100$  m and in the blue line for the case of  $\phi = -10^\circ$  and  $d = 600$  m. The data indicate that the adjustment effect of  $\Delta T$  decreases by

33% for every degree increase in  $FSL$  for any cases in this range.

When  $d = 100$  m, regardless of the  $FSL$ , the increment and decrement of  $\Delta T$  are similar. As  $d$  gradually increases, the increment of  $\Delta T$  begins to decrease, while the decrement of  $\Delta T$  gradually increases. When  $d = 500$  m, the decrement of  $\phi = -10^\circ$  is almost twice as much as the increment of  $\phi = +10^\circ$ .

### 3.2. Drawback Distance Responding

The response relationship between the rotation effect and the drawback distance is shown in **Figure 6**. In the case of reverse rotation, the rotation effect becomes more and more pronounced as  $d$  increases, and the linearity becomes better, but the variation of  $\Delta T$  with  $d$  is not obvious. When  $\phi = -10^\circ$ , the gap between  $d = 100$  m and  $d = 600$  m is just about 0.8 m. While in the case of forward rotation of  $\phi = +10^\circ$ , the difference between  $d = 100$  m and  $d = 600$  m is approximately 1.1 m. The distribution is looser than in the case of reversal. However, on the contrary, as  $d$  increases, the rotation effect gets weaker and weaker, and the linearity deteriorates.

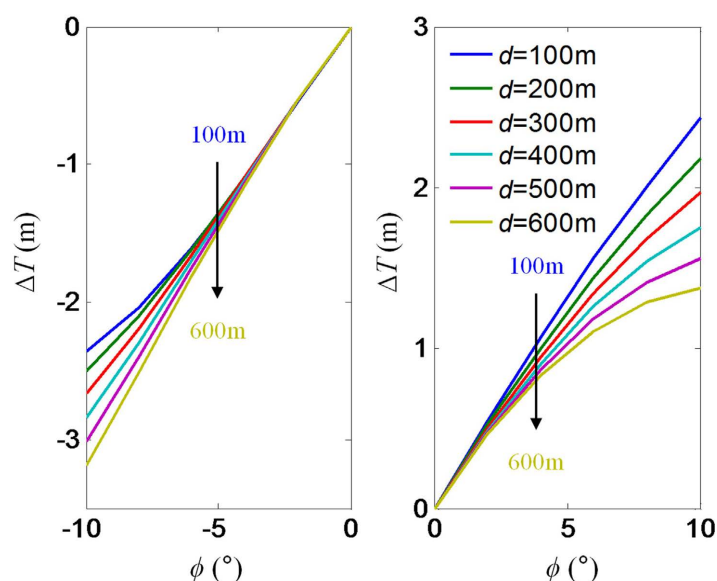


**Figure 6.** (Color online)  $\Delta T$  responds to  $\phi$  with a series of  $d$  for  $FSL = 0^\circ$ . The left figure responds to the negative rotation angle  $\phi$ , and the right figure responds to the positive rotation angle  $\phi$  with  $d = 100$  m to 600 m.

The comparison of the rotation effects of forward and reverse by a maximum of ten degrees is summarized in **Table 2**. As analyzed in the previous **Figure 5**,  $\Delta T$  is basically consistent at 100 meters. As the distance increases, the proportion increases. As the distance increases, the proportion becomes increasingly disparate. When  $d = 200$  m, the proportion increases by 18%. When  $d = 500$  m, it has already doubled. When  $d$  arrives 600 meters, the proportion increases by another 40%. The impact of  $FSL$  on the proportion can be ignored. It can be considered that  $FSL$  is independent relative to  $d$ .

**Table 2.**  $\Delta T$  ratio of forward and reverse rotation by 10 degrees.

$\Delta T_{-10^\circ}/\Delta T_{+10^\circ}$	100 m	200 m	300 m	400 m	500 m	600 m
$FSL = -2^\circ$	-0.96	-1.14	-1.36	-1.61	-1.93	-2.32
$FSL = -1^\circ$	-0.96	-1.14	-1.35	-1.61	-1.93	-2.32
$FSL = 0^\circ$	-0.97	-1.14	-1.36	-1.62	-1.93	-2.33
$FSL = 1^\circ$	-0.97	-1.15	-1.36	-1.62	-1.94	-2.35
$FSL = 2^\circ$	-0.99	-1.17	-1.41	-1.67	-1.99	-2.40

### 3.3. Rotating Angle Responding

To fully study the response characteristics of  $\Delta T$  with respect to  $d$  under different rotation angles  $\phi$ , the normalized proportional relationship distributions are given for ten kinds of rotation angles, as listed in **Figure 7**.

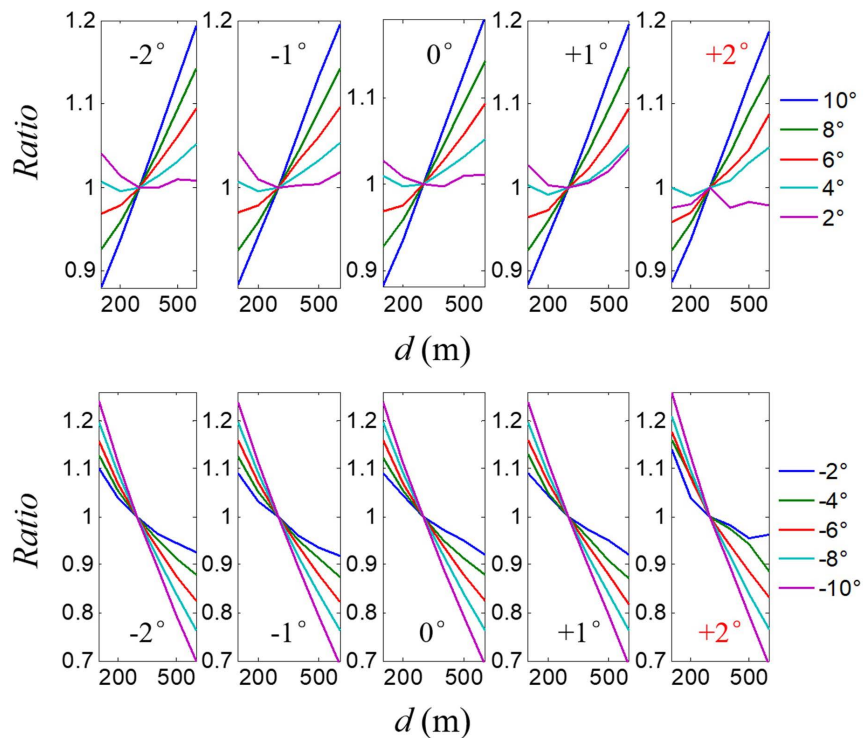


**Figure 7.** (Color online) Normalized  $\Delta T$  relative to  $d = 300$  meters responds to  $d$  with a series of  $\phi$  in different  $FSL$ . The curves at the top represent forward rotation, and the curves at the bottom represent reverse rotation.

In the case of forward rotation, the larger the rotation angle  $\phi$ , the better the linear behavior. Meanwhile, the larger  $\phi$  corresponds to the larger slope of the curves and the better linear features. When the angle is small, linearity gradually deteriorates, even the monotonicity behavior appears to disappear, and fluctuations appear when  $\phi = 2^\circ$ , especially in the case of  $FSL = 2^\circ$ . In the case of reverse rotation, similarly, the large  $\phi$  embodies the good linearity. However, the larger the  $d$ , the worse the rotation effect. The ratio indicates that the effect in  $d = 100$  m

is 120% than that of  $d = 300$  m. By comparison, the rotation effect in  $d = 600$  m falls to 70% than that of  $d = 300$  m.

When  $FSL = 2^\circ$ , the linearity of both small-angle forward and reverse rotation is poor. This phenomenon originates from the slope approaching the Glide Path angle, and the signal becomes unstable.

#### 4. Summary/Conclusions

A special method of adjustment of TCH by antenna rotation is investigated concerning a series of longitudinal zone factors. TCH can be raised or lowered freely and accurately by electrically adjustable rotation. The regularity of variation related to backward distance ( $d$ ) and forward slope ( $FSL$ ) is revealed digitally and intensively. TCH increases with the increase of  $d$ . And TCH increases with the decrease of  $FSL$ . Both of these factors show good linear behavior. The variation of  $\Delta T$  with  $d$  is monotonic,  $\Delta T$  increases as  $d$  increases, and reflects a strong correlation of  $\Delta T$  with  $FSL$ . The adjustment effect of  $\Delta T$  decreases by 33% for every degree increase in  $FSL$ . And  $FSL$  also has the same impact on TCH adjustment. When  $FSL$  arrives at two degrees, the angle is closer to the glide slope angle, and an abnormal situation occurs with a small-angle  $\phi$  rotation. More complex situations, such as lateral terrain and multipath from buildings, will be studied in the future.

#### Conflicts of Interest

The author declares no conflicts of interest regarding the publication of this paper.

#### References

- [1] Kwasiowska, A., Grabowski, M., Sedláčková, A.N. and Novák, A. (2023) The Influence of Visibility on the Opportunity to Perform Flight Operations with Various Categories of the Instrument Landing System. *Sensors*, **23**, Article 7953. <https://doi.org/10.3390/s23187953>
- [2] Novák, A., Havel, K. and Janovec, M. (2017) Measuring and Testing the Instrument Landing System at the Airport Zilina. *Transportation Research Procedia*, **28**, 117-126. <https://doi.org/10.1016/j.trpro.2017.12.176>
- [3] Sun, J. (2024) Specification for Instrument Landing System. *Exploration of Educational Management*, **2**, 107-111.
- [4] Xu, J., Ye, J., Liang, F., Li, Y. and Lin, H. (2021) Simulation Analysis and Research on the Influence of Buildings on a Glide Path Antenna. 2021 *International Conference on Computer Technology and Media Convergence Design (CTMCD)*, Sanya, 23-25 April 2021, 63-66. <https://doi.org/10.1109/ctmcd53128.2021.00022>
- [5] Qu, C.Q. (2018) Brief Introduction of a New Kind of Glide Path Antenna. *Open Journal of Antennas and Propagation*, **6**, 60-72. <https://doi.org/10.4236/ojapr.2018.63006>
- [6] Abd-Elaty, E., Zekry, A., El-Agoz, S. and Helaly, A.M. (2022) Underlay Spectrum Sharing with L-Band Distance Measuring Equipment for Aeronautical Communications. *Wireless Personal Communications*, **128**, 2363-2377. <https://doi.org/10.1007/s11277-022-10045-0>
- [7] Qu, C.Q. (2025) Digital Analysis on Antenna Tilt in Complex Field Based on Artifi-

- cial Intelligence. *Journal of Physics: Conference Series*, **3004**, Article ID: 012099. <https://doi.org/10.1088/1742-6596/3004/1/012099>
- [8] Normarc (2018) Normarc7000B Training Manual. Normarc, 23-24.
- [9] Normarc (2016) Normarc 3545 M-Array Glide Path Antenna System Instruction manual.
- [10] ICAO (2006) Annex 10, Aeronautical Telecommunications, Vol. I. ICAO.
- [11] Kock, N. and Hadaya, P. (2016) Minimum Sample Size Estimation in PLS-SEM: The Inverse Square Root and  $\gamma$ -Exponential Methods. *Information Systems Journal*, **28**, 227-261. <https://doi.org/10.1111/isj.12131>